Transition metal dopants essential for producing ferromagnetism in metal oxide nanoparticles

Lydia M. Johnson,[1] Aaron Thurber,[1] Joshua Anghel,[1] Maryam Sabetian,[1] Mark H. Engelhard,[2] Dmitri A. Tenne,[1] Charles B. Hanna,[1] and Alex Punnoose[1,*]

[1]*Department of Physics, Boise State University, Boise, Idaho 83725, USA*

[2]*Environmental Molecular Sciences Laboratory, Pacific Northwest National Laboratory, Richland, Washington 99352, USA*

(Received 3 November 2009; revised manuscript received 29 June 2010; published 13 August 2010)

Recent claims that ferromagnetism can be produced in nanoparticles of metal oxides without the presence of transition metal dopants have been challenged in this work by investigating 62 high-quality well-characterized nanoparticle samples of both undoped and Fe-doped (0–10 % Fe) ZnO. The undoped ZnO nanoparticles showed zero or negligible magnetization without any dependence on the nanoparticle size. However, chemically synthesized $Zn_{1-x}Fe_xO$ nanoparticles showed clear ferromagnetism, varying systematically with Fe concentration. Furthermore, the magnetic properties of $Zn_{1-x}Fe_xO$ nanoparticles showed strong dependence on the reaction media used to prepare the samples. The zeta potentials of the $Zn_{1-x}Fe_xO$ nanoparticles prepared using different reaction media were significantly different, indicating strong differences in the surface structure.

DOI: 10.1103/PhysRevB.82.054419 PACS number(s): 75.75.−c, 81.07.−b, 75.50.Pp

I. INTRODUCTION

Development of new magnetic materials by doping semiconducting metal oxides with transition metal (TM) ions has been reported extensively since the prediction of room-temperature ferromagnetism (RTFM) in these oxides.[1–3] However, some recent reports claimed that RTFM can be produced in metal oxides without any TM dopants, if prepared in nanoparticle (NP) (Refs. 4–7) or thin-film forms.[8–11] For example, based on experiments using an extensive set of metal oxides including ZnO, Sundaresan *et al.*[4] have reported that undoped NP (size 7–30 nm) samples of these oxides displayed ferromagnetism at room temperature while their bulk counterparts were diamagnetic. They argued that the ferromagnetism resulted from the exchange interactions between localized electron spin moments produced by the oxygen vacancies on the NP surface. Further, Garcia *et al.*[6] reported that by modifying the surface through the capping of 10 nm NPs with three different organic molecules, they could achieve variations in the magnetic properties of undoped ZnO NP. A combined theoretical and experimental study by Fernandez *et al.*[11] argued that RTFM is possible in undoped ceria. Similar magnetism has also been reported in other nonmagnets such as gold, silicon, and graphite.[12–15] In order to determine the likelihood of these claims, we prepared an extensive series of NP samples of zinc oxide with well defined sizes in the 4–20 nm range with (38 samples) and without (24 samples) Fe dopant, and investigated these samples thoroughly using a wide range of experimental techniques. The samples were synthesized by a chemical route that allows systematic variation of size, Fe dopant concentration, and reaction solvent to control the surface structure. If the magnetism is a result of active spin moments on the particle surface, the sample magnetization must increase systematically with decreasing particle size. Our studies did not show any systematic dependence of the saturation magnetization with NP size, rather, appreciable RTFM was observed in the NP samples only if they contained Fe dopants. The observed magnetization varies strongly with Fe doping concentration and the surface structure. Interestingly, none of the undoped NP samples showed any appreciable ferromagnetism. These results suggest that the ferromagnetism observed in undoped metal oxide NPs is likely of impurity origin. While intentional alteration of NP surface structure can affect the strength of observed magnetization, TM dopants are necessary for the origination of appreciable RTFM.

II. EXPERIMENTAL DETAILS

Zinc oxide NPs were prepared using similar chemical hydrolysis methods,[16] one in diethylene glycol (DEG) and the other in denatured ethanol solutions, hereafter referred to as ZnO-I and ZnO-II, respectively. The samples were prepared from the same zinc acetate dihydrate precursor. Since two different solvents were used, the NPs should have different surface structure/groups depending on whether the particles are made by method I or method II. By varying the hydrolysis ratio (water: zinc acetate), ZnO-I samples were prepared in the 4–20 nm range, and by varying the reaction time, ZnO-II samples were prepared in the 4–9 nm range. In order to study the effect of TM dopant on the magnetic properties, samples were also prepared with iron ions doped using coprecipitation employing zinc and iron acetates in the hydrolysis process. The dopant concentration x is given by the molar ratio of [Fe]/([Fe]+[Zn]). Samples were characterized and investigated in detail using x-ray diffraction (XRD), magnetometry, transmission electron microscopy (TEM), Zeta potential measurements, and x-ray photoelectron spectroscopy (XPS).

XRD spectra were recorded at room temperature on a Philips X'Pert x-ray diffractometer with a Cu $K\alpha$ source ($\lambda = 1.5418$ Å) in Bragg-Brentano geometry. The loose powder samples were leveled in the sample holder to ensure a smooth surface and mounted on a fixed horizontal sample plane. Data analyses were carried out using profile fits of selected individual XRD peaks.

Zeta potentials of the powdered samples of undoped ZnO NPs and $Zn_{1-x}Fe_xO$ NPs were measured in nanopure water as a function of pH with a Malvern Zetasizer NanoZS. The temperature was equilibrated to 25 °C, and the pH was var-

ied in the 6–12 range using 1.0 N HCl and 1.0 N NaOH prior to collecting the data. At least eight data collections per run were performed on three separate aliquots of the ZnO suspension for each sample.

High-resolution TEM analysis was carried out on a JEOL JEM-2100HR microscope with a specified point-to-point resolution of 0.23 nm. The operating voltage of the microscope was 200 kV. Image processing was carried out using the DIGITAL MICROGRAPH software from Gatan (Pleasant, California, USA).

For XPS measurements, the Fe-doped ZnO powders were mounted onto the XPS sample holder by pressing onto double sided Nichiban tape inside a 3 mm diameter Moly finger mask. XPS spectra were recorded using a Physical Electronics Quantum 2000 Scanning ESCA Microprobe available at the Pacific Northwest National Laboratory. This system uses a focused monochromatic Al $K\alpha$ x-ray (1486.7 eV) source and a spherical section analyzer. The instrument has a 16 element multichannel detector. The x-ray beam used was a 100 W, 100 μm diameter beam that was rastered over a 1.3 mm by 0.2 mm rectangle on the sample. The x-ray beam is incident normal to the sample and the photoelectron detector was at 45° off-normal. The high energy resolution photoemission spectra were collected using a pass energy of 46.95 eV. For the Ag $3d_{5/2}$ line, these conditions produced full-width at half maximum of better than 0.98 eV. The binding energy scale is calibrated using the Cu $2p_{3/2}$ feature at 932.62 ± 0.05 eV and Au $4f$ at 83.96 ± 0.05 eV for known standards. The samples experienced variable degrees of charging. Low-energy electrons at ~1 eV, 20 μA and low-energy Ar^+ ions were used to minimize this charging. The spectra shown here were charge referenced using the C 1s line at 284.8 eV.

Magnetic measurements were carried out at room temperature using a LakeShore model 7404 vibrating sample magnetometer by tightly packing powder samples placed in a clear plastic drinking straw. The magnetization data was recorded as a function of applied magnetic field up to ± 1 T The data reported here were corrected for the background signal from the sample holder (clear plastic drinking straw) with diamagnetic susceptibility $\chi = -4.1 \times 10^{-8}$ emu/Oe.

III. RESULTS AND DISCUSSION

XRD was employed to investigate the structural properties and crystallite size, and to rule out the presence of any unwanted impurity phases. The representative XRD patterns shown in Fig. 1(a) display only the wurtzite ZnO phase with no indication of other phases even in the sample with the highest Fe concentration of 10%. Since the XRD system used in this work has a detection ability of chemical phases with more than 1.5% (determined from XRD measurements of a physical mixture of ZnO and α-Fe_2O_3), this clearly rules out the presence of any crystalline iron oxides or other binary oxides. The XRD peak positions of both ZnO-I and ZnO-II showed gradual changes with Fe doping, revealing interesting variations in the lattice parameters a and c and lattice volume V, determined using suitable pairs of (100), (102), (110), and (103) peaks, as shown in Fig. 1(b). This

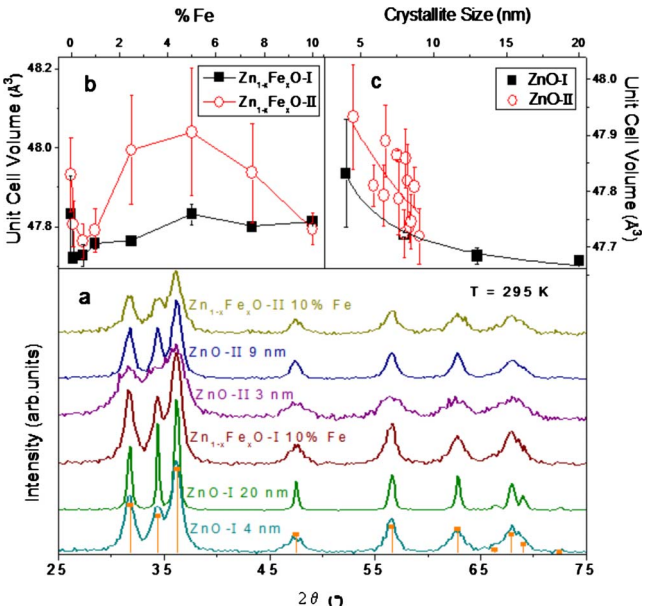

FIG. 1. (Color online) Panel (a) shows sample XRD patterns of ZnO-I, ZnO-II, $Zn_{1-x}Fe_xO$-I, and $Zn_{1-x}Fe_xO$-II NPs. Drop lines indicate the expected XRD peak positions and relative intensities. Also shown is the variation in unit-cell volume V for (b) $Zn_{1-x}Fe_xO$-I and $Zn_{1-x}Fe_xO$-II NPs as a function of x and (c) ZnO-I and ZnO-II NPs as a function of L.

provides evidence for increasing incorporation of Fe ions in ZnO crystallites since the ZnO lattice volume initially increases due to Fe doping up to 5%. This can be understood qualitatively considering the sizes and charges of the ions and their local coordinations when Fe ions substitute for Zn^{2+} ions. This might also require rearrangement of neighboring oxygen and/or Zn^{2+} ions for charge neutrality. The relatively mild, but opposite changes in the lattice volume for >5% doping indicates additional incorporation of dopant ions in interstitial sites as has been reported in some host systems causing somewhat similar structural changes in the lattice parameters.[17,18] Analysis of lattice parameters for the undoped NPs of both ZnO-I and ZnO-II samples showed a gradual increase in the unit-cell volume V with decreasing particle size L as shown in Fig. 1(c). A similar increase in V with decreasing L has been observed in other oxide NP systems also due to their large surface to volume ratio.[19]

Average crystallite size L of the undoped ZnO NPs and the doped $Zn_{1-x}Fe_xO$ NPs were calculated using the width of the (102) peak and the Scherrer relation, $L = \frac{0.9\lambda}{B \cos\theta}$ (where θ is the peak position, λ is the x-ray wavelength and peak width $B = (B_m^2 - B_s^2)^{1/2}$ was estimated using the measured peak width B_m and the instrumental width B_s). The crystallite sizes of all the $Zn_{1-x}Fe_xO$-I and $Zn_{1-x}Fe_xO$-II NP were 6.8 ± 0.6 nm and 6.9 ± 0.2 nm, respectively. Average L for undoped ZnO-I samples were ~4, 8, 13, and 20 nm and ZnO-II NP were ~3.9, 4.4, 5.6, 6.9, 7.8, 8.3, and 9.0 nm. TEM images (Fig. 2) of Fe-doped $Zn_{1-x}Fe_xO$ NPs and pure ZnO NPs smaller than 10 nm showed nearly spherical particles. For ZnO NPs larger than 10 nm, the particles become somewhat elongated. Particle size distribution analysis of the samples conducted using TEM images confirmed that the

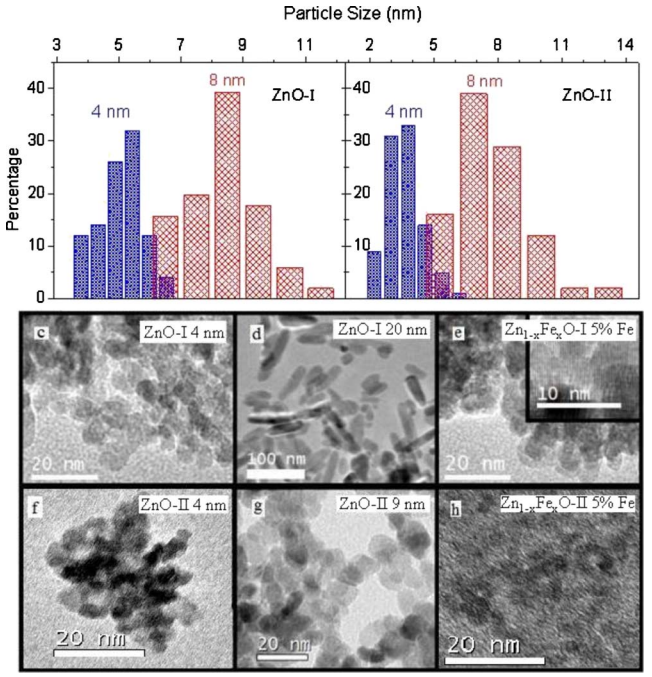

FIG. 2. (Color online) Top panels show size distribution plots of NPs with average size of 4 nm and 8 nm for (a) ZnO-I and (b) ZnO-II. The middle row of panels show TEM images of ZnO-I NPs of (c) 4 nm and (d) 20 nm size, and (e) $Zn_{1-x}Fe_xO$-I for $x=0.05$. The bottom row of panels show TEM images of ZnO-II NPs of (f) 4 nm and (g) 9 nm size, and (h) $Zn_{1-x}Fe_xO$-II for $x=0.05$.

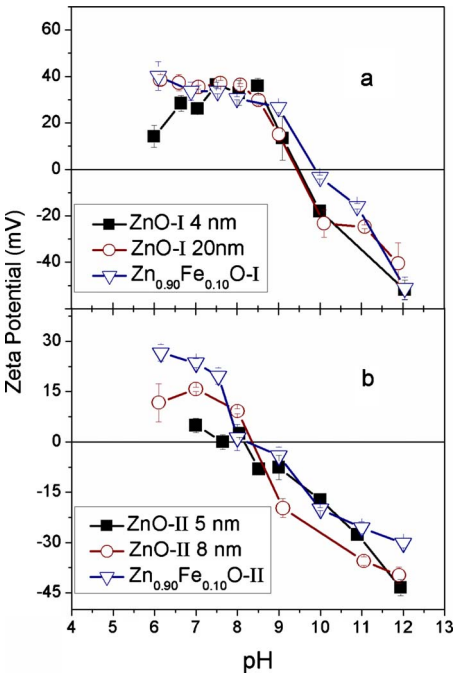

FIG. 3. (Color online) Zeta potentials of 5 mM NP concentration in nanopure water as a function of pH for (a) 4 and 20 nm sized ZnO-I and $Zn_{1-x}Fe_xO$-I with $x=0.10$ and (b) 4 and 9 nm sized ZnO-II, and $Zn_{1-x}Fe_xO$-II with $x=0.10$.

particle size variations in all the samples employed here are within approximately ± 4 nm (see Fig. 2).

Unlike bulk materials, NPs have large surface to volume ratio and the NP surface consists of uncompensated charged ions. ZnO-I and ZnO-II NP were synthesized in two different solution media, namely, DEG and ethanol respectively, and therefore their surface structure and charge are expected to be different. To obtain insight into their surface structure and charge, zeta potentials of the powdered samples of undoped ZnO NPs and Fe-doped $Zn_{1-x}Fe_xO$ NPs suspended in nanopure water were measured as a function of pH. Zeta potential at pH of ~7.5 showed differing surface charge for samples prepared in DEG and ethanol with ZnO-I samples averaging to $\sim+40\pm5.0$ mV and ZnO-II samples giving less than half that at $\sim+15\pm12.0$ mV. Zeta potentials of ZnO-I and ZnO-II NPs as a function of pH for different crystallite sizes are shown in Fig. 3. Zeta potentials of all the $Zn_{1-x}Fe_xO$-I NPs were similar at $+33\pm1.4$ mV suggesting that the Fe doping did not modify the surface charge significantly. This is true for the $Zn_{1-x}Fe_xO$-II set also although with a lower zeta potential of $+18\pm2.1$ mV. Thus, these measurements clearly demonstrate that the zeta potentials and therefore the surface structure of the NP samples prepared in DEG medium (set I) and ethanol medium (set II) are significantly different.

XPS measurements were employed to investigate the possible presence of any iron oxides in the $Zn_{1-x}Fe_xO$ crystallites. The Fe $3p_{1/2}$ XPS spectral region of $Zn_{1-x}Fe_xO$-II NPs with different x is shown in Fig. 4. The core level Fe $3p_{1/2}$ peak was observed at ~54.7 eV and 55.2 eV for $Zn_{1-x}Fe_xO$-I and $Zn_{1-x}Fe_xO$-II NPs, respectively. These binding energy values are clearly different from the binding energies of Fe $3p_{1/2}$ peak expected for most common iron oxides such as magnetite (53.9 eV), hematite (55.7 eV), and maghemite (55.7 eV).[20,21] This rules out the presence of these common iron oxides in $Zn_{1-x}Fe_xO$ samples and also clearly demonstrates the difference in the atomic environment surrounding the incorporated Fe ions in $Zn_{1-x}Fe_xO$ from that of these oxides. Thus, the XPS data clearly suggest that the Fe peaks observed from the $Zn_{1-x}Fe_xO$ samples are not arising from any maghemite, hematite, or magnetite inclusions in the samples.

Room temperature magnetization M vs magnetic field H measurements were carried out on all the samples. The resulting hysteresis loops were analyzed to determine the satu-

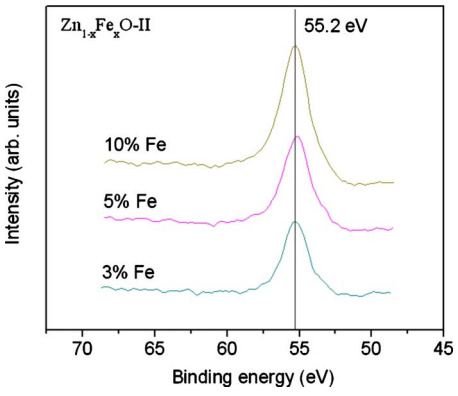

FIG. 4. (Color online) Plot showing the Fe $3p_{1/2}$ XPS spectral region of $Zn_{1-x}Fe_xO$-II NPs with different x indicated. The vertical line is positioned at 55.2 eV.

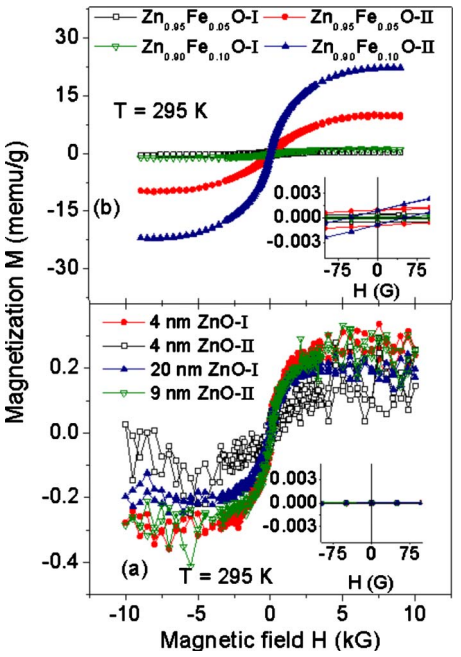

FIG. 5. (Color online) Room temperature M vs H measurements on powders of selected (a) ZnO-I and ZnO-II samples and (b)$Zn_{1-x}Fe_xO$-I and $Zn_{1-x}Fe_xO$-II NP samples. Insets show the low field regions of the same data.

ration magnetization M_s, remanence M_r, and coercivity H_c of these samples. A few representative hysteresis loops of doped and undoped ZnO-I and ZnO-II are shown in Fig. 5. The undoped ZnO-I and ZnO-II NP samples showed closed or very weak hysteresis loops, with M_s in the 0–1memu/g, M_r in the 0–0.05 memu/g, and H_c in the 0–300 G range. The hysteresis loop parameters showed that varying size of the ZnO NP samples prepared using both methods (ZnO-I and ZnO-II) in the 4–20 nm range did not result in systematic changes in M_s [Fig. 6(a)], H_c [Fig. 6(b)], or M_r. If the magnetism is arising from the surface of undoped NPs as other reports have claimed,[4–7] the observed weak magnetism should have varied systematically with particle size. The random variation in the magnetization of the undoped ZnO with decreasing particle size therefore indicates that the ferromagnetism is most likely arising from weak impurities present in these samples that were so low in concentration to escape detection in the characterization studies. The extremely large surface of NPs is more likely to adsorb impurity atoms/ions compared to that of their bulk counterparts. Note that ferromagnetism has been reported in metal oxides doped with even $<0.5\%$ of TM ions.[18] Our NP samples of pure undoped ZnO were prepared in the 4–20 nm range, which covers the sizes used by all the studies[4–7] that reported ferromagnetism in undoped ZnO NPs, and measurements were conducted on 24 independently synthesized ZnO NP samples to ensure that our results are statistically significant.

Doping ZnO NPs with Fe had dramatic effects on the magnetic properties, showing a systematic increase in M_s with increasing Fe content, as shown in Fig. 6(c). This result clearly suggests that TM dopants are essential to produce ferromagnetism in ZnO. The $Zn_{1-x}Fe_xO$-II samples showed much stronger magnetization compared to $Zn_{1-x}Fe_xO$-I. For

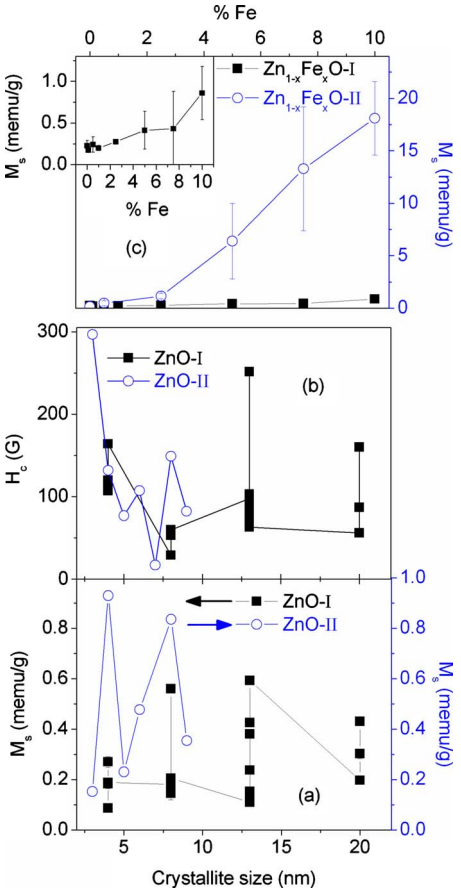

FIG. 6. (Color online) (a) Variation in the saturation magnetization M_s vs particle size L plotted for both ZnO-I and ZnO-II NPs, (b) Variation in the coercivity H_c vs particle size L plotted for both ZnO-I and ZnO-II NPs, and (c) M_s vs Fe concentration of $Zn_{1-x}Fe_xO$-I and $Zn_{1-x}Fe_xO$-II NPs. Inset shows expansion of the same $Zn_{1-x}Fe_xO$-I data.

example, for 10% Fe concentration, the $Zn_{1-x}Fe_xO$-II samples displayed 20 times stronger M_s than $Zn_{1-x}Fe_xO$-I. Since these two sets of samples were prepared following a similar procedure, but in different reaction media, the only difference expected is in their surface structure as evidenced from the significantly different zeta potentials. Thus, it can be concluded that the difference in the surface structure of $Zn_{1-x}Fe_xO$-I and $Zn_{1-x}Fe_xO$-II is responsible for the observed difference in ferromagnetism between the two sets. Note that the reason for the low magnetic moment per Fe ion (5.64×10^{-4} μ_B/ion in $Zn_{1-x}Fe_xO$-I and 3.57×10^{-3} μ_B/ion in $Zn_{1-x}Fe_xO$-II) is not well understood but may be due to DMS behavior or ferromagnetic inclusions.

One might argue that the observed magnetism might be due to superparamagnetism resulting from isolated DMS NP or possible nanoscale non-DMS FM inclusions. However, the magnetization data shown in Fig. 5(b) (inset) clearly displays an open loop, and all Fe doped samples consistently displayed coercivity in the 30–240 G range. Presence of clear coercivity rules out the possibility of superparamagnetism and supports a ferromagnetic origin. If the superparamagnet is below its blocking temperature, ferromagneticlike behavior with open hysteresis loop is possible. However, this

will require a blocking temperature well above room temperature. Further, regarding the possibility of some non-DMS ferromagnetic/superparamagnetic impurity phase being present in the sample, our detailed characterization studies using XRD and XPS have clearly ruled out the possible presence of metallic Fe, its magnetic oxides or Fe-Zn binary oxides. Samples doped with Fe% as high as 10% also showed no impurity phases. Further, random presence of such impurities is unlikely to produce a systematic increase in magnetization with increasing Fe%.

IV. CONCLUSION

In summary, the detailed experimental studies described above on well-characterized samples of undoped and Fe doped ZnO NPs clearly demonstrate that while surface structure can influence the strength of observed magnetism, TM dopants are necessary to produce an appreciable ferromagnetism in ZnO NPs. The NP samples of pure undoped ZnO prepared in the 4–20 nm range, which covers the sizes used in all the recent reports claiming ferromagnetism in undoped ZnO NPs, showed zero or negligible magnetism. The observed magnetization did not show a systematic increase with decreasing particle size (i.e., increasing particle surface) of the ZnO NPs, thus demonstrating that defects present increasingly in NPs because of their large surface to volume ratio are not solely responsible for the observed ferromagnetism in undoped metal oxide NPs. On the other hand, similar ZnO NPs synthesized with a TM ion (Fe) doped intentionally using identical synthesis procedures showed ferromagnetism and their magnetization varied systematically with Fe% (0–10 % range), thus underlining that TM dopants are essential for ferromagnetism in metal oxides. These results make one wonder if the magnetism observed in undoped oxide NPs (especially those prepared using similar synthesis methods) is truly intrinsic or if it results from weak impurity/TM inclusions that are too low to be detected in most characterization tools. This work also compared the effect of different surface structures on the magnetism of Fe doped ZnO NPs and indeed observed significant differences in M_s (up to 20 times) suggesting that the NP surface structure plays a key role in the modification of magnetic properties. This work thus provides a method to improve the ferromagnetic properties of TM doped metal oxides through careful tailoring of the surface structure.

ACKNOWLEDGMENTS

This work was supported in part by the NSF-CAREER program (Grant No. DMR-0449639), DoE-EPSCoR program (Grant No. DE-FG02-04ER46142), ARO under Grant No. W911NF-09-1-0051, NSF-MRI under Awards No. 0722699 and No. 0521315, and NSF-RUI (Grant No. DMR-0840227). A portion of the research described in this paper was performed in the Environmental Molecular Sciences Laboratory, a national scientific user facility sponsored by the Department of Energy's Office of Biological and Environmental Research and located at Pacific Northwest National Laboratory.

*Corresponding author; apunnoos@boisestate.edu

[1] T. Dietl, A. Haury, and Y. M. d'Aubigne, Phys. Rev. B **55**, R3347 (1997).
[2] K. Sato and H. Katayama-Yoshida, Physica B **308-310**, 904 (2001).
[3] T. Dietl, H. Ohno, F. Matsukura, J. Cibert, and D. Ferrand, Science **287**, 1019 (2000).
[4] A. Sundaresan, R. Bhargavi, N. Rangrajan, U. Siddesh, and C. N. R. Rao, Phys. Rev. B **74**, 161306 (2006).
[5] D. Gao, Z. Zhang, J. Fu, Y. Xu, J. Qi, and D. Xue, J. Appl. Phys. **105**, 113928 (2009).
[6] M. A. Garcia, J. M. Merino, E. Fernndez Pinel, A. Quesada, J. de la Venta, M. L. Ruíz Gonzlez, G. R. Castro, P. Crespo, J. Llopis, J. M. Gonzlez-Calbet, and A. Hernando, Nano Lett. **7**, 1489 (2007).
[7] S. Kumar, Y. J. Kim, B. H. Koo, S. Gautam, K. H. Chae, R. Kumar, and C. G. Lee, Mater. Lett. **63**, 194 (2009).
[8] J. M. D. Coey, M. Venkatesan, P. Stamenov, C. B. Fitzgerald, and L. S. Dorneles, Phys. Rev. B **72**, 024450 (2005).
[9] H. H. Hong, I. Sakai, N. Poirot, and V. Brize, Phys. Rev. B **73**, 132404 (2006).
[10] S. D. Yoon, Y. Chen, A. Yang, T. L. Goodrich, X. Zuo, K. Ziemer, C. Vittoria, and V. G. Harris, J. Magn. Magn. Mater. **309**, 171 (2007).
[11] V. Fernandes, R. J. O. Mossanek, P. Schio, J. J. Klein, A. J. A. de Oliveira, W. A. Ortiz, N. Mattoso, J. Varalda, W. H. Schreiner, M. Abbate, and D. H. Mosca, Phys. Rev. B **80**, 035202 (2009).
[12] P. Esquinazi, D. Spemann, R. Hohne, A. Setzer, K. H. Khan, and T. Bultz, Phys. Rev. Lett. **91**, 227201 (2003).
[13] G. Kopnov, Z. Vager, and R. Naaman, Adv. Mater. **19**, 925 (2007).
[14] P. Crespo, R. Litrán, T. C. Rojas, M. Multigner, J. M. de la Fuente, J. C. Sánchez-López, M. A. García, A. Hernando, S. Penadés, and A. Fernández, Phys. Rev. Lett. **93**, 087204 (2004).
[15] I. Carmeli, G. Leitus, R. Naaman, S. Reich, and Z. Veger, J. Chem. Phys. **118**, 10372 (2003).
[16] K. M. Reddy, K. Feris, J. Bell, D. G. Wingett, C. Hanley, and A. Punnoose, Appl. Phys. Lett. **90**, 213902 (2007).
[17] J. Hays, K. M. Reddy, N. Graces, M. H. Engelhard, V. Shutthanandan, N. Giles, C. Wang, S. Thevuthasan, and A. Punnoose, J. Phys.: Condens. Matter **19**, 266203 (2007).
[18] J. Hays, A. Punnoose, R. Baldner, M. H. Engelhard, J. Peloquin, and K. M. Reddy, Phys. Rev. B **72**, 075203 (2005).
[19] A. Punnoose, H. Magnone, M. S. Seehra, and J. Bonevich, Phys. Rev. B **64**, 174420 (2001).
[20] N. S. McIntyre and D. G. Zetaruk, Anal. Chem. **49**, 1521 (1977).
[21] A. Punnoose, J. Hays, A. Thurber, M. H. Engelhard, R. K. Kukkadapu, C. Wang, V. Shutthanandan, and S. Thevuthasan, Phys. Rev. B **72**, 054402 (2005).